

PhD Thesis Defense



Estudio de la Interacción de Flujos Múltiples de Fuentes Astrofísicas, Aplicada a los Proplyds Clásicos de la Nebulosa de Orión

Presents: M.C Jorge Alejandro Tarango Yong

PhD Advisor: Dr. William Henney

Tutorial Committee: Dr. Javier Ballesteros, Dr. Luis Zapata

February 27, 2019

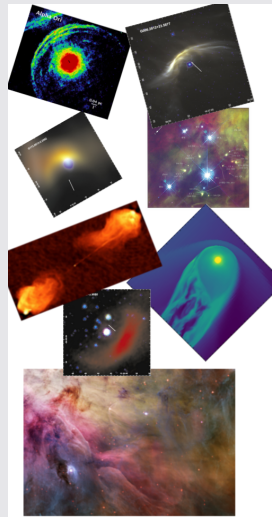
Index

- 1 Introduction**
- 2 Bow Shocks in the ISM**
- 3 Orion Nebula**
- 4 Fundamental Concepts**
- 5 Thin Shell Model**
- 6 Results Obtained for the Classical Proplyds in Orion Nebula**
- 7 Summary and Conclusions**

- 1** Introduction
- 2** Bow Shocks in the ISM
- 3** Orion Nebula
- 4** Fundamental Concepts
- 5** Thin Shell Model
- 6** Results Obtained for the Classical Proplyds in Orion Nebula
- 7** Summary and Conclusions

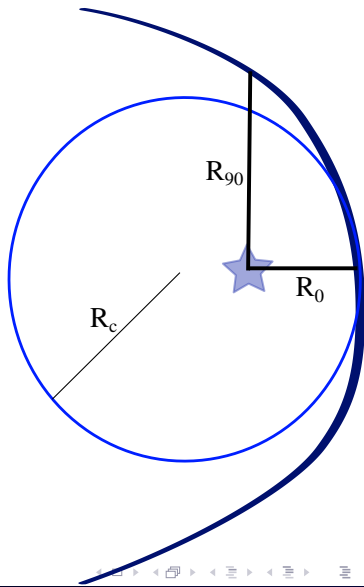
Motivation of this work

Bow shocks occur in many kinds of astrophysical scenarios, from galactic to planetary scales. In this work we develop a mathematical tool for characterizing cylindrically symmetric, geometrically thin and optically thin bow shocks based into their geometrical shape and how is oriented respect the plane of sky.

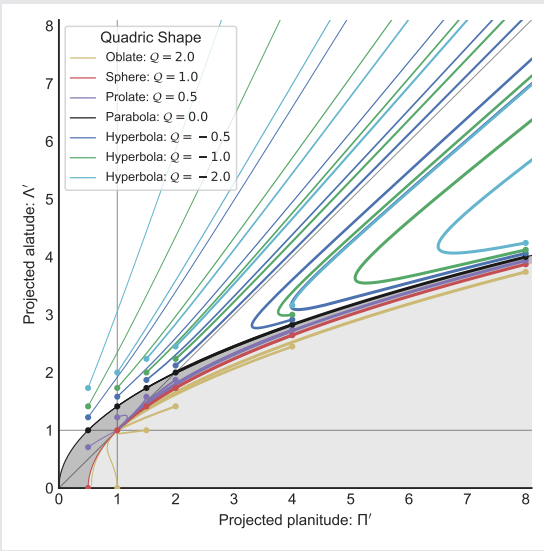


Motivation of this work

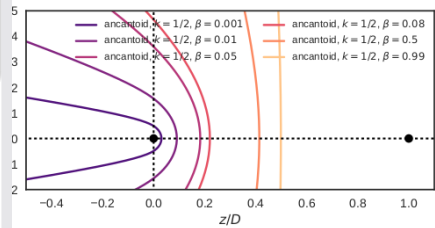
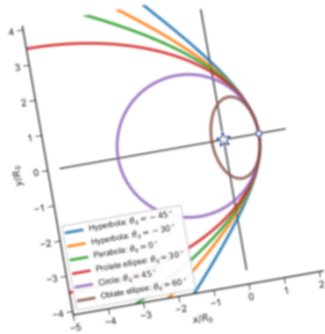
We do this by measuring two non-dimensional parameters: the planitude $\Pi = R_c/R_0$ and the alatitude $\Lambda = R_{90}/R_0$, easily measurable from observations.



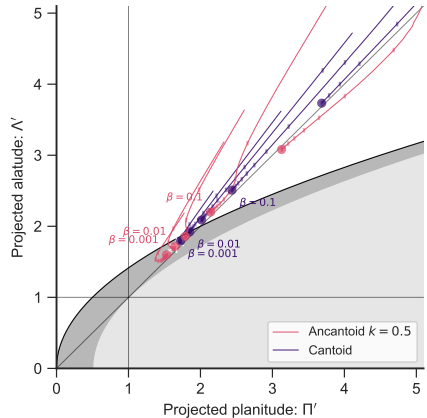
We called it the Λ' – Π' diagram (Tarango Yong & Henney, 2018).



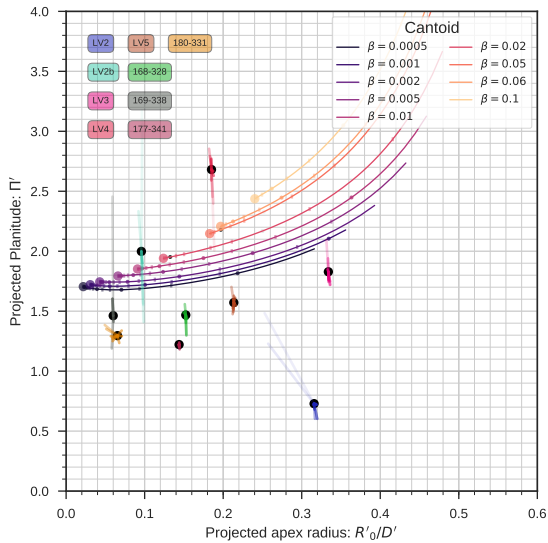
Then we apply this tool to the simplest mathematical surfaces: the quadrics of revolution (Goldman, 1983; Gfrerrer & Zsombor-Murray, 2009) and to a simple model for winds interaction: the Thin Shell Model (Cantó et al., 1996).



Then we apply this tool to the simplest mathematical surfaces: the quadrics of revolution (Goldman, 1983; Gfrerrer & Zsombor-Murray, 2009) and to a simple model for winds interaction: the Thin Shell Model (Cantó et al., 1996).



And finally compare the thin shell model against observations of the classical proplyds of the Trapezium in the core of the Orion Nebula in a similar diagram.

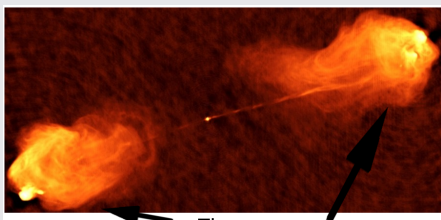


- 1** Introduction
- 2** Bow Shocks in the ISM
- 3** Orion Nebula
- 4** Fundamental Concepts
- 5** Thin Shell Model
- 6** Results Obtained for the Classical Proplyds in Orion Nebula
- 7** Summary and Conclusions

Bow Shocks in the ISM

Bow shocks are emission arcs produced when some fluid interacts at supersonic speeds with another object. Some astrophysical examples seen in the Interstellar Medium (ISM) are:

- **Jets working surfaces**
- Magnetosphere interaction with stellar wind
- Stellar Bow shocks
 - AGB stars and red supergiants
 - Runaway O stars
 - Proplyds
 - T Tauri stars
 - Neutron stars

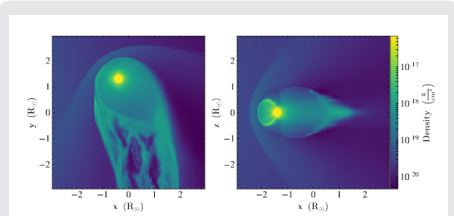


Cygnus A (Perley et al., 1984)

Bow Shocks in the ISM

Bow shocks are emission arcs produced when some fluid interacts at supersonic speeds with another object. Some astrophysical examples seen in the Interstellar Medium (ISM) are:

- Jets working surfaces
- **Magnetosphere interaction with stellar wind**
- Stellar Bow shocks
 - AGB stars and red supergiants
 - Runaway O stars
 - Proplyds
 - T Tauri stars
 - Neutron stars



Density of material flowing from a Hot Jupiter through magnetosphere interacting with stellar wind (Daley-Yates & Stevens, 2018).

Bow Shocks in the ISM

Bow shocks are emission arcs produced when some fluid interacts at supersonic speeds with another object. Some astrophysical examples seen in the Interstellar Medium (ISM) are:

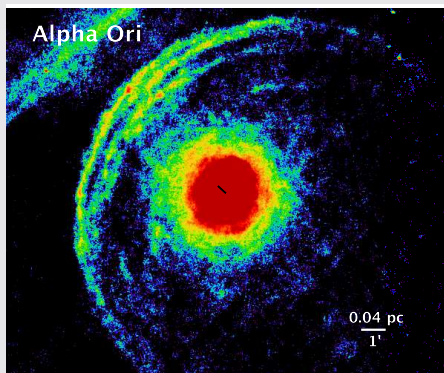
- Jets working surfaces

- Magnetosphere interaction with stellar wind

- Stellar Bow shocks

- **AGB stars and red supergiants**

- Runaway O stars
 - Proplyds
 - T Tauri stars
 - Neutron stars

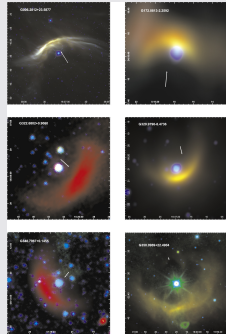


Observation of a “Fermata” type bow shock at $70 \mu\text{m}$ produced by the interaction of the strong wind of a red supergiant (α Ori) with the ISM (Cox et al., 2012).

Bow Shocks in the ISM

Bow shocks are emission arcs produced when some fluid interacts at supersonic speeds with another object. Some astrophysical examples seen in the Interstellar Medium (ISM) are:

- Jets working surfaces
- Magnetosphere interaction with stellar wind
- Stellar Bow shocks
 - AGB stars and red supergiants
 - **Runaway O stars**
 - Proplyds
 - T Tauri stars
 - Neutron stars

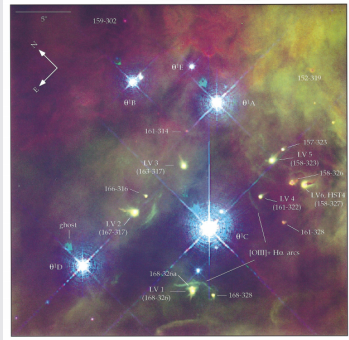


Observations of prototypical examples of “Bow shock nebulae” by Spitzer or WISE produced by runaway stars interacting with the ISM (red: 20 or 22 μ m, green: 8 or 12 μ m, blue: 4.5 μ m)(Kobulnicky et al., 2016).

Bow Shocks in the ISM

Bow shocks are emission arcs produced when some fluid interacts at supersonic speeds with another object. Some astrophysical examples seen in the Interstellar Medium (ISM) are:

- Jets working surfaces
- Magnetosphere interaction with stellar wind
- Stellar Bow shocks
 - AGB stars and red supergiants
 - Runaway O stars
 - **Proplyds**
 - T Tauri stars
 - Neutron stars



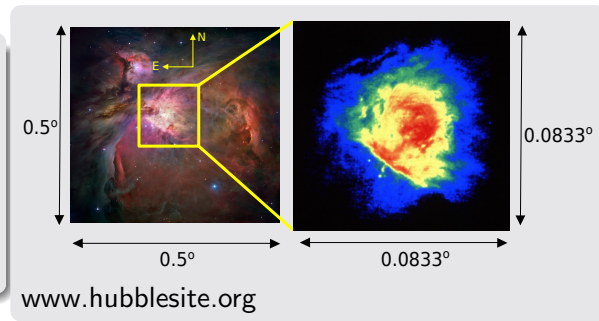
The Classical proplyds in the core of the trapezium in Orion Nebula also show a bow shock by the HST (red is $[N\ II]$, green is $H\alpha$ and blue is $[O\ I]$) (Bally et al., 1998).

► Return button

- [1] Introduction**
- [2] Bow Shocks in the ISM**
- [3] Orion Nebula**
- [4] Fundamental Concepts**
- [5] Thin Shell Model**
- [6] Results Obtained for the Classical Proplyds in Orion Nebula**
- [7] Summary and Conclusions**

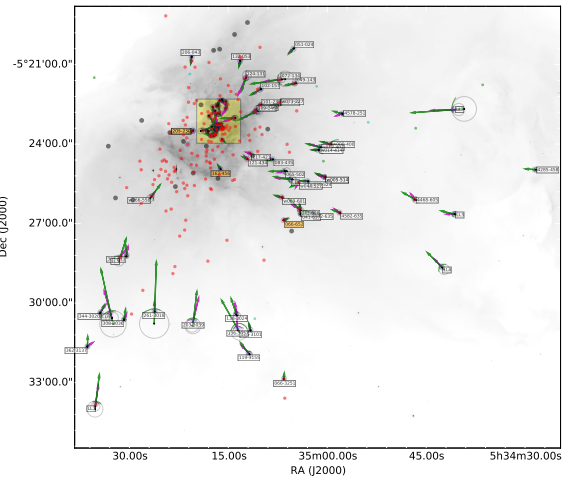
Orion Nebula

The Orion Nebula is the nearest H II region (~ 414 pc, Menten et al. (2007)), where massive star formation can be studied with high resolution observations.



Proplyds in Orion Nebula

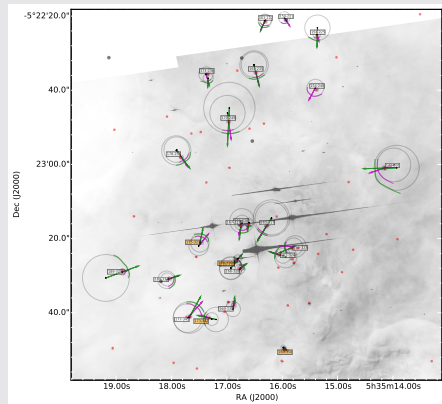
About 70 arcs have been detected within Orion Nebula (Gutiérrez-Soto, 2015), many of them are produced by proplyds.



Map of bow shocks in Orion Nebula (Gutiérrez-Soto, 2015)

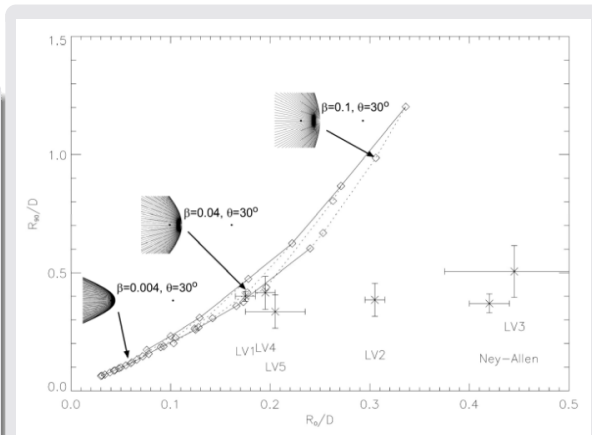
Proplyds in Orion Nebula

About 70 arcs have been detected within Orion Nebula (Gutiérrez-Soto, 2015), many of them are produced by proplyds.



Map of bow shocks in Orion Nebula (Trapezium zoomed) (Gutiérrez-Soto, 2015)

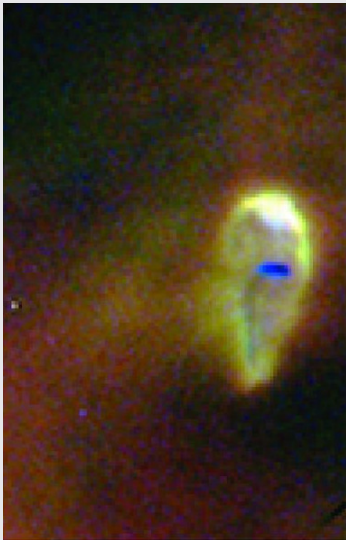
Some of the nearest proplyds to θ^1 Ori C were previously observed by Bally et al. (1998) [► Go to image](#) and Robberto et al. (2005) in mid infrared and their shape analyzed using the Thin Shell Model from (Cantó et al., 1996), but some proplyds don't fit at all.



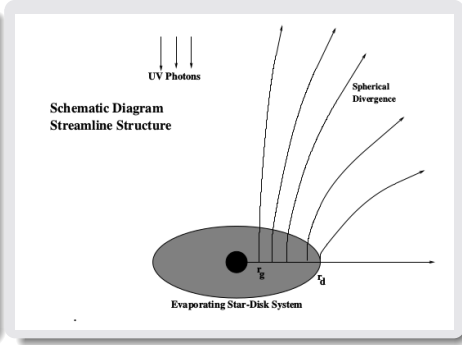
Apparent shape of some proplyds (in black points) compared with the thin shell model of (Cantó et al., 1996) (open dots and lines) in a R_{90}/D vs R_0/D diagram (Robberto et al., 2005).

Photoevaporated wind in proplyds

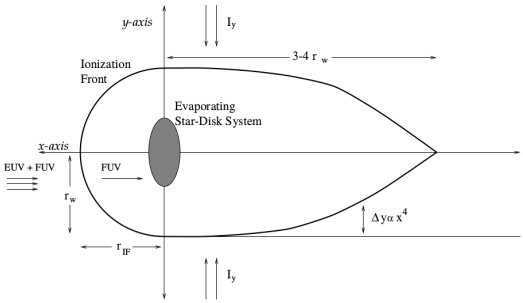
Proplyds are bright structures with cometary shape which are the result of the photoevaporation of a protoplanetary disk (hence the name) due to a strong source of ultraviolet radiation (e.g a massive star).



The incident UV radiation photoevaporates the gas in the protoplanetary disk, which becomes a spherical flow due to pressure gradients. Only the gas located at $r > r_g = \frac{GM_*}{a^2}$ (where M_* is the mass of the central star and a is the speed of sound of the gas) can escape from the disk.



The head is shaped by the incident UV radiation from the massive star, forming a D type Ionization Front, while the tail is shaped by diffuse radiation.



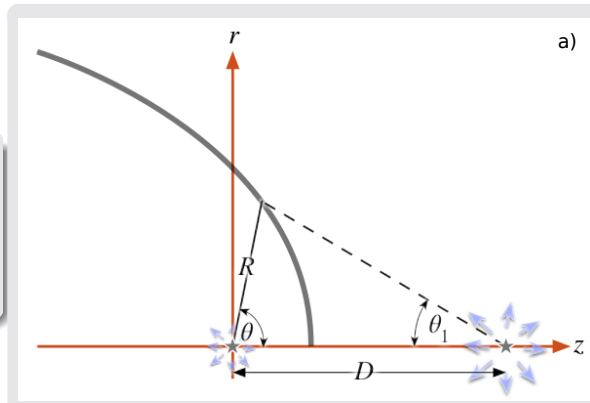
(Johnstone et al., 1998)

- 1** Introduction
- 2** Bow Shocks in the ISM
- 3** Orion Nebula
- 4** Fundamental Concepts
- 5** Thin Shell Model
- 6** Results Obtained for the Classical Proplyds in Orion Nebula
- 7** Summary and Conclusions

General Considerations

For our model for the two-winds interaction which forms a bow shock we consider two main scenarios:

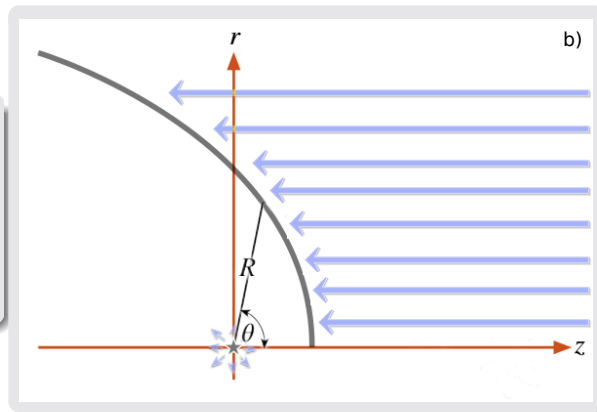
A weaker wind placed at the origin, and a stronger wind separated by a distance D from the former one.



General Considerations

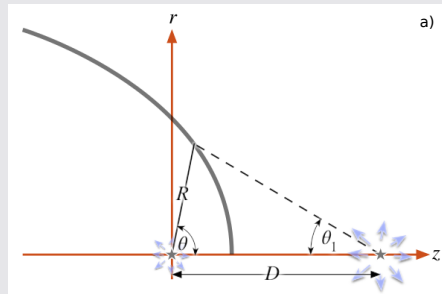
For our model for the two-winds interaction which forms a bow shock we consider two main scenarios:

The second scenario is a spherical, isotropic wind placed at the origin interacting with a plane-parallel flow with constant density



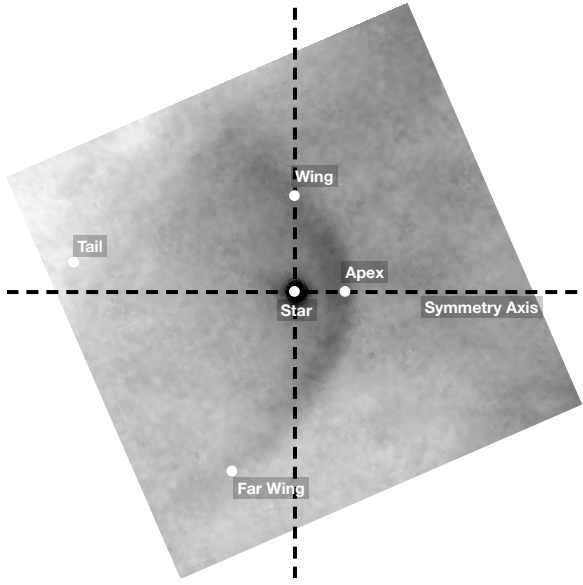
General Considerations

The shape of the bow shock is determined by the function $R(\theta, \phi)$, where (θ, ϕ) are the usual polar and azimuthal angle. Since the bow shocks are (ideally) cylindrically symmetric, then the bow shock shape may be given by $R(\theta)$, and is enough to represent it with a bidimensional curve with constant ϕ . In the two spherical wings scenario, the polar angle measured from the second source is θ_1 . The symmetry axis of the bow shock is aligned with the z axis.



Bow shocks terminology

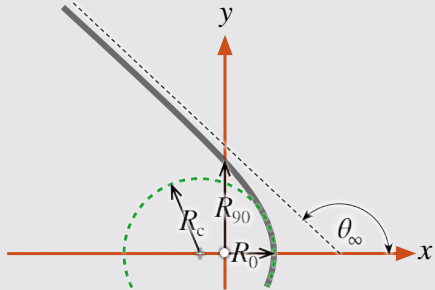
- The minimal radius of the bow shock is called “head” or apex.
- The far sides of the apex are called “wings”



Planitude and Alatitude

To characterize the shape of a given bow shock we use a set of parameters:

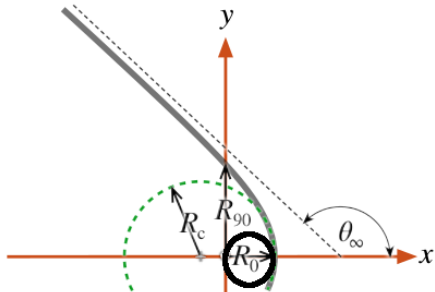
- The radius at the apex, called R_0 , which gives us the bow shock physical scale, and is defined as the minimum of $R(\theta)$
- The asymptotic angle θ_∞ of the far wings (which usually is not measurable)
- The planitude $\Pi \equiv R_c/R_0$, which measures how flat is the apex
- The alatitude $\Lambda \equiv R_{90}/R_0$, which measures how open the wings are



Planitude and Alatitude

To characterize the shape of a given bow shock we use a set of parameters:

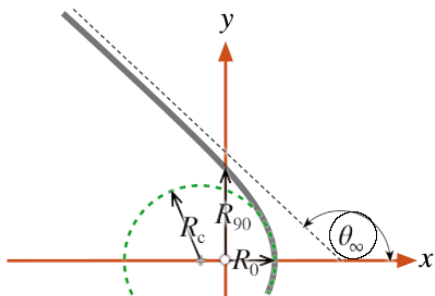
- **The radius at the apex, called R_0 , which gives us the bow shock physical scale, and is defined as the minimum of $R(\theta)$**
- The asymptotic angle θ_∞ of the far wings (which usually is not measurable)
- The planitude $\Pi \equiv R_c/R_0$, which measures how flat is the apex
- The alatitude $\Lambda \equiv R_{90}/R_0$, which measures how open the wings are



Planitude and Alatitude

To characterize the shape of a given bow shock we use a set of parameters:

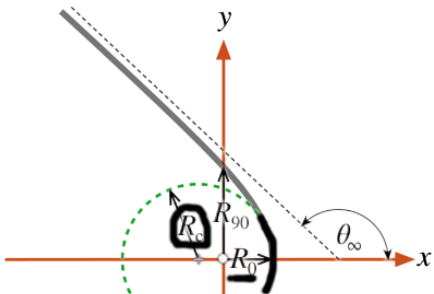
- The radius at the apex, called R_0 , which gives us the bow shock physical scale, and is defined as the minimum of $R(\theta)$
- **The asymptotic angle θ_∞ of the far wings (which usually is not measurable)**
- The planitude $\Pi \equiv R_c/R_0$, which measures how flat is the apex
- The alatitude $\Lambda \equiv R_{90}/R_0$, which measures how open the wings are



Planitude and Alatitude

To characterize the shape of a given bow shock we use a set of parameters:

- The radius at the apex, called R_0 , which gives us the bow shock physical scale, and is defined as the minimum of $R(\theta)$
- The asymptotic angle θ_∞ of the far wings (which usually is not measurable)
- **The planitude $\Pi \equiv R_c/R_0$, which measures how flat is the apex**
- The alatitude $\Lambda \equiv R_{90}/R_0$, which measures how open the wings are



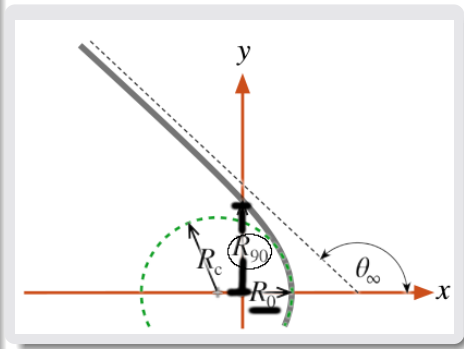
► To see the algebraic expressions, click [HERE](#)

Planitude and Alatitude

To characterize the shape of a given bow shock we use a set of parameters:

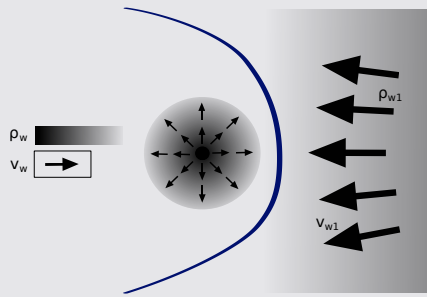
- The radius at the apex, called R_0 , which gives us the bow shock physical scale, and is defined as the minimum of $R(\theta)$
- The asymptotic angle θ_∞ of the far wings (which usually is not measurable)
- The planitude $\Pi \equiv R_c/R_0$, which measures how flat is the apex
- **The alatitude $\Lambda \equiv R_{90}/R_0$, which measures how open the wings are**

► To see the algebraic expressions, click [HERE](#)



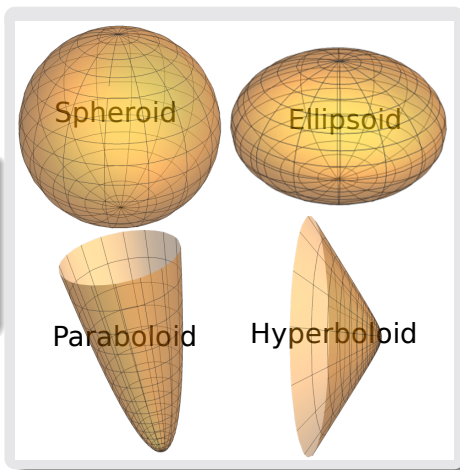
Winds Properties

The relevant parameters of the winds are the terminal velocity v and the mass loss rate \dot{M} , related to the density ρ . Following (Cantó et al., 1996), we use the sub-index w for the weaker wind properties and the sub-index $w1$ for the stronger wind properties.



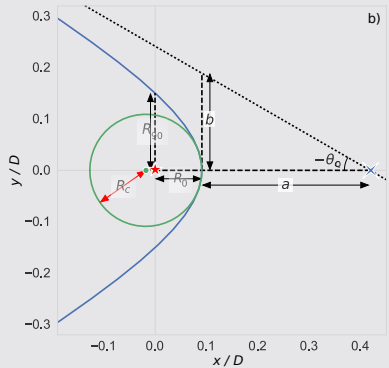
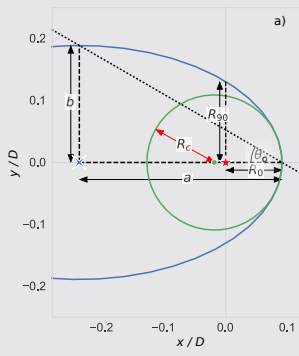
Quadrics of Revolution

Quadrics of Revolution are the surfaces of revolution of conic sections. May be a good and useful approximation to more complex surfaces



Quadratics of Revolution: basic definitions

Our conic section symmetry axis is aligned with the x axis, and the center is displaced from the origin by distance called x_0 . The physical scale of the conic section is set using the semi-major and semi-minor axis a and b .



► To see the parametrization of quadrics click [HERE](#)

Quadratics of Revolution: basic definitions

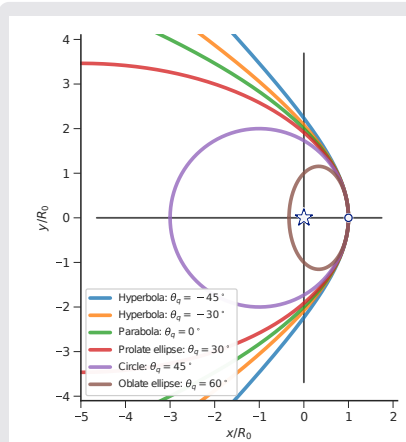
The eccentricity is replaced with the quadratics parameter \mathcal{Q} defined as:

$$\mathcal{Q} = \sigma \frac{b^2}{a^2}$$

Or the angle θ_q :

$$\tan \theta_q = \sigma \frac{b}{a}$$

Positive values of \mathcal{Q} are associated with closed curves (i.e. ellipsoids), and $\mathcal{Q} \leq 0$ are associated with open curves.



Quadrics of Revolution: basic definitions

The parameters set (a, x_0, Q) is enough to characterize the curve, but for future applications the set (R_0, Π, Λ) is more useful. So, the transformation between the two sets is given by:

$$R_0 = x_0 + \sigma a$$

$$\Pi = \frac{aQ}{a + \sigma x_0}$$

$$\Lambda = \left(Q \frac{a - \sigma x_0}{a + \sigma x_0} \right)^{1/2}$$

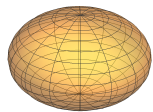
Finally, the quadrics parameter (and thus the kind of quadric) may be computed from the planitude and alatitude as follows:

$$Q = 2\Pi - \Lambda^2$$

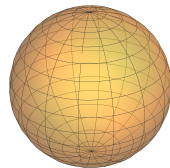
Quadratics of revolution: basic definitions

This implies that the relative values of (Π, Λ) determines the type of conic.

$$2\Pi > \Lambda^2$$



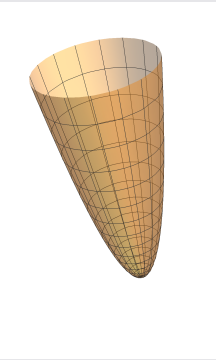
$$2\Pi - \Lambda^2 = 1$$



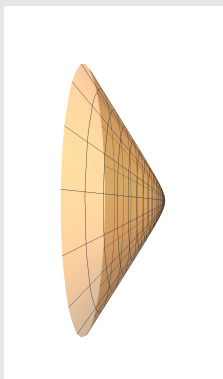
Quadratics of revolution: basic definitions

This implies that the relative values of (Π, Λ) determines the type of conic.

$$2\Pi = \Lambda^2$$

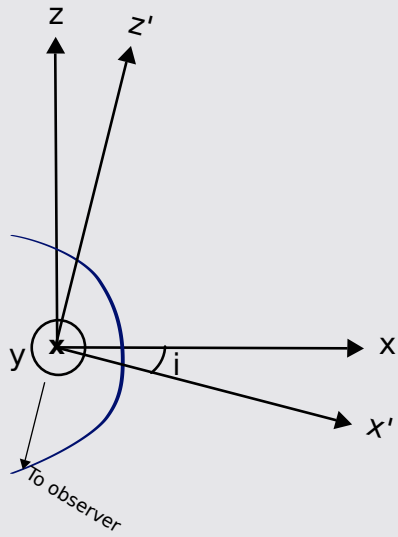


$$2\Pi < \Lambda^2$$



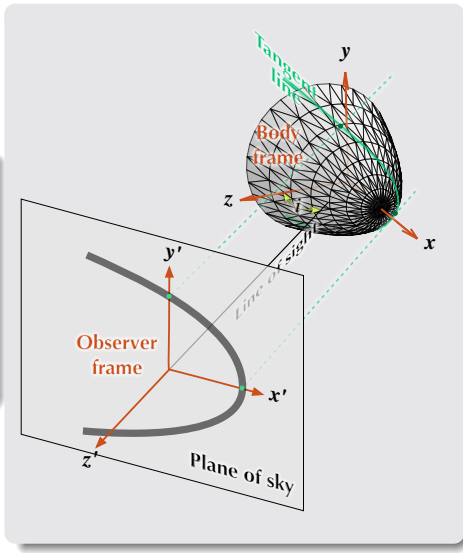
Projection Onto the Plane of Sky

We consider two reference frames in cartesian coordinates: The non primed reference system, where the x axis is aligned with the symmetry axis of the bow shock, is called the body frame. And the primed system, where the $-z$ axis points toward the observer, is called the observer frame. The x and x' axis forms an angle called *inclination* and is denoted as i .



Projection Onto the Plane of Sky

The “tangent line” (the edge) of a bidimensional surface geometrically thin and optically thin is visible through limb brightening as an arc. The shape of the visible arc under these conditions varies with the inclination.



Projection Onto the Plane of Sky

Tridimensional shape in the body frame: Rotation along the x axis of the bidimensional curve.

$$\begin{pmatrix} x \\ y \\ z \end{pmatrix} = A_x(\phi) \begin{pmatrix} R(\theta) \cos \theta \\ R(\theta) \sin \theta \\ 0 \end{pmatrix} \Rightarrow \begin{pmatrix} x \\ y \\ z \end{pmatrix} = \begin{pmatrix} R(\theta) \cos \theta \\ R(\theta) \sin \theta \cos \phi \\ R(\theta) \sin \theta \sin \phi \end{pmatrix}$$

Transformation between body frame and observer frame

$$\begin{pmatrix} x' \\ y' \\ z' \end{pmatrix} = A_y(i) \begin{pmatrix} x \\ y \\ z \end{pmatrix} \Rightarrow \begin{pmatrix} x' \\ y' \\ z' \end{pmatrix} = \begin{pmatrix} x \cos i - z \sin i \\ y \\ z \cos i + x \sin i \end{pmatrix}$$

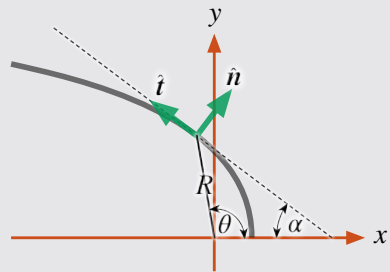
► Go to Matrix Expression

Projection Onto the Plane of Sky

Normal and tangent unit vectors

We define the unit vectors \hat{t} and \hat{n} as the tangent and normal vectors to the surface at certain point (to check the expression of each one go to [this slide](#)). The tangent line of the surface at the inclination i is such that the line of sight is orthogonal to the normal unitary vector:

$$\hat{n} \cdot \hat{z}' = 0$$



Projection Onto the Plane of Sky

The angle ϕ which fulfills the tangent line condition is such that:

$$\sin \phi_T = \tan i \frac{1 + \omega \tan \theta}{\omega - \tan \theta}$$

where:

$$\omega = \frac{1}{R} \frac{dR}{d\theta}$$

Since z'_T is not a linear function of θ , then the projected shape does not lie in a plane.

With this, the projected shape is given by:

$$\begin{pmatrix} x'_T \\ y'_T \\ z'_T \end{pmatrix} = \begin{pmatrix} R(\theta)(\cos \theta \cos i - \sin \theta \sin \phi_T \sin i) \\ R(\theta) \sin \theta (1 - \sin^2 \phi_T)^{1/2} \\ R(\theta)(\cos \theta \sin i + \sin \theta \sin \phi_T \cos i) \end{pmatrix}$$

Projected Alatitude and Planitude

For an arbitrary inclination, the tangent line does not exist for $\theta < \theta_0$, where:

$$\tan \theta_0 = \frac{|\tan i| + \omega(\theta_0)}{1 - \omega(\theta_0)|\tan i|}$$

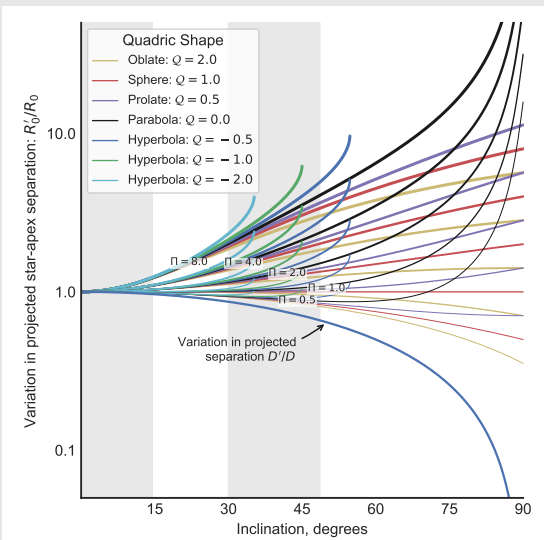
For “open” shapes, when i is large enough, there is no tangent line for any θ .

- The projected radius at the apex R'_0 is computed as x'_T such that $y'_T = 0$:
- R'_{90} is computed as y'_T such that $x'_T = 0$
- And the projected radius of curvature is computed as the intrinsic planitude but in the observer frame.

[To see the equations for each radii, click HERE](#)

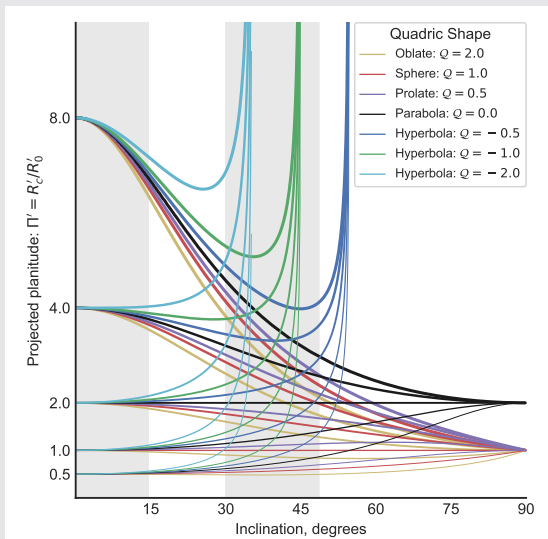
Projected Alatitude and Planitude of Quadrics of Revolution

Projected apex radius



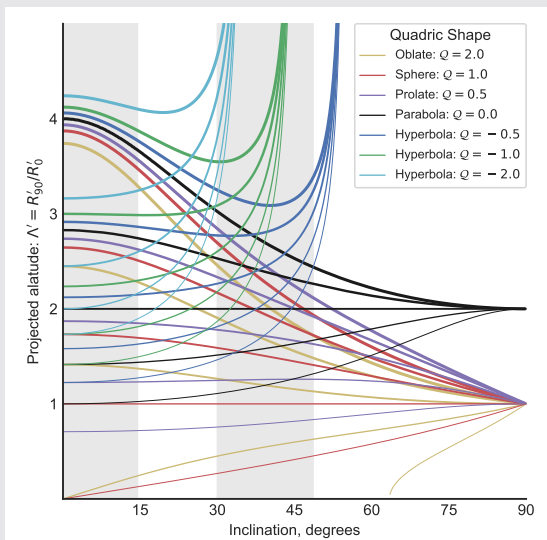
Projected Alatitude and Planitude of Quadrics of Revolution

Projected planitude



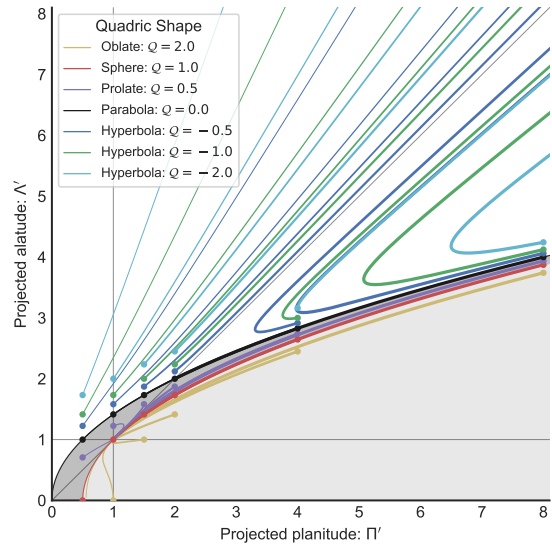
Projected Alatitude and Planitude of Quadrics of Revolution

Projected alatitude



The Λ – Π Diagram

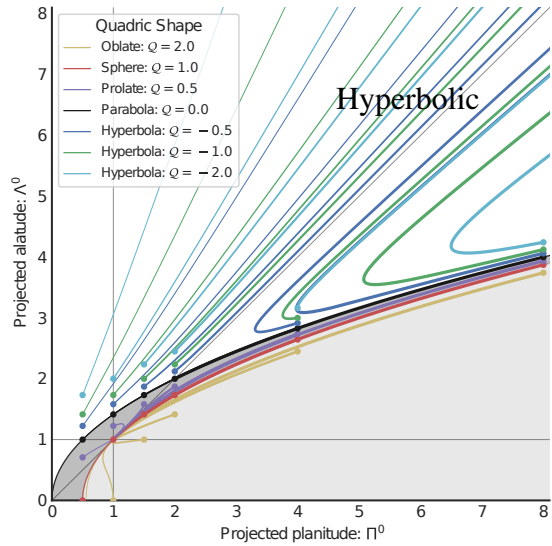
Comparing the projected alatitude against the projected planitude we identify three regions:



The Λ – Π Diagram

Comparing the projected alatitude against the projected planitude we identify three regions:

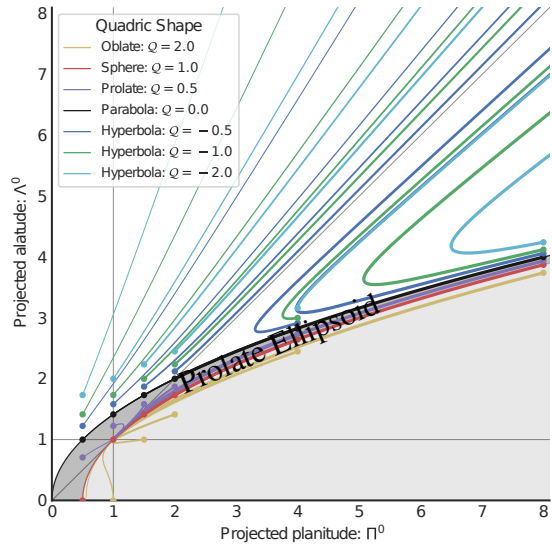
- The upper region where the hyperboloid shapes lie.



The Λ – Π Diagram

Comparing the projected alatitude against the projected planitude we identify three regions:

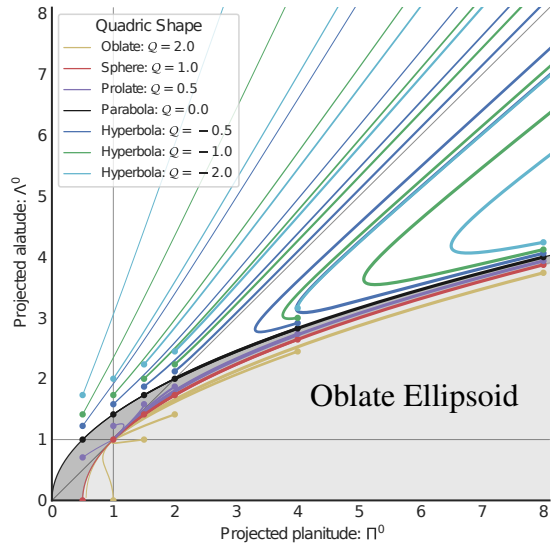
- A narrow intermediate region for the prolate ellipsoids.



The Λ – Π Diagram

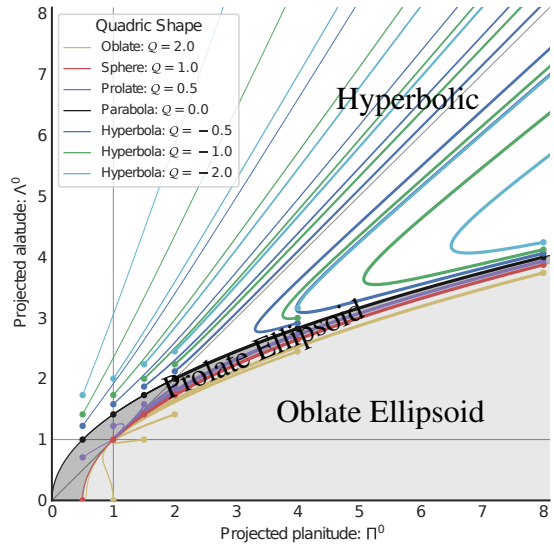
Comparing the projected alatitude against the projected planitude we identify three regions:

- The lower region for the oblate ellipsoids.



The Λ – Π Diagram

The interfaces between regions correspond to the paraboloid and the spheroid.



- [1] Introduction**
- [2] Bow Shocks in the ISM**
- [3] Orion Nebula**
- [4] Fundamental Concepts**
- [5] Thin Shell Model**
- [6] Results Obtained for the Classical Proplyds in Orion Nebula**
- [7] Summary and Conclusions**

Introduction

A (little) more realistic model to compute the shape of the bow shock come from steady state hydrodinamical models for two winds interaction in the thin shell limit in stationary state. For example Cantó et al. (1996).

© THE ASTROPHYSICAL JOURNAL, 469:729–733, 1996 October 1
© 1996. The American Astronomical Society. All rights reserved. Printed in U.S.A.

EXACT ALGEBRAIC SOLUTIONS OF THE THIN-SHELL TWO-WIND INTERACTION PROBLEM

J. CANTÓ,¹ A. C. RAGA,¹ AND F. P. WILKIN²

Received 1996 February 21; accepted 1996 April 23

ABSTRACT

We have developed a formalism based on considerations of linear and angular momentum conservation for solving axisymmetric, steady, “thin-shell” problems, which is applicable to problems of interactions of nonaccelerated flows. This formalism yields a system of algebraic equations that can be solved to obtain the shape of the thin shell, its mass surface density, and the velocity along the shell. We first use this approach to obtain the solution (obtained with a somewhat different approach by Wilkin 1996) to the problem of an isotropic stellar wind interacting with a plane-parallel stream. Second, we find an exact (implicit) and approximate (explicit) analytic solution to the problem of the interaction of two isotropic stellar winds.

Our solution of the two-wind problem is a step forward from previous numerical solutions based on a ram-pressure balance argument since it is analytic and, furthermore, includes centrifugal effects. This solution has clear applications to problems of interacting winds in binary stars as well as in young stellar objects.

Subject headings: hydrodynamics — ISM: bubbles — shock waves — stars: mass loss

1. INTRODUCTION

The problem of the interaction of two hypersonic, constant-velocity, isotropic stellar winds is of clear astrophysical interest and has been studied in some detail in the past. Stevens, Blondin, & Pollock (1992) carried out numerical simulations of this two-wind problem using the full gasdynamic equations and considered both the adiabatic and radiative cases. The first thin-shell analyses of this problem were carried out by Huang & Weigert (1982) and by Girard & Wilson (1987). Kallrath (1991) and Dyson, Hartquist, & Biro (1993) numerically obtained the surface of ram-pressure balance between the two winds,

Winds symmetry

The symmetry of the winds is classified into three scenarios:

Cantoid bow shocks

Isotropic inner wind



Isotropic outer wind



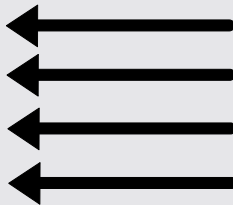
Winds symmetry

Wilkinoid bow shocks

Isotropic inner wind



Plane-parallel stream



Winds symmetry

The previous two scenarios were discussed previously in Cantó et al. (1996), but we add a third scenario:

Ancantoid bow shocks

Anisotropic hemispherical wind

The density of the inner wind is proportional to $\cos^k \theta$, where θ is the polar angle and k is the power index.
 $k = 0$.



Isotropic outer wind



Winds symmetry

Anisotropic hemispherical wind

$k = 1/2$, adequated for [proplyds](#).



Isotropic outer wind



Winds symmetry

Anisotropic hemispherical wind

$k = 3.$



Isotropic outer wind

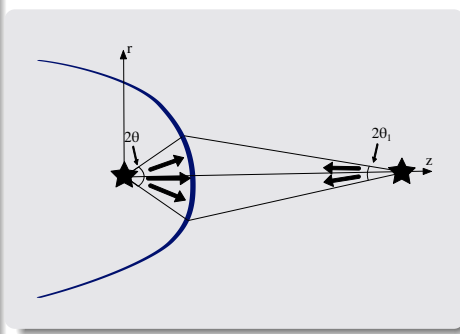


Discontinuity Contact Shape

The shape of the discontinuity contact $R(\theta)$ is given by equation (6) of (Cantó et al., 1996):

$$R = \frac{\dot{J}_w + \dot{J}_{w1}}{(\dot{\Pi}_{wr} + \dot{\Pi}_{wrl})\cos \theta - (\dot{\Pi}_{wz} + \dot{\Pi}_{wzl})\sin \theta}$$

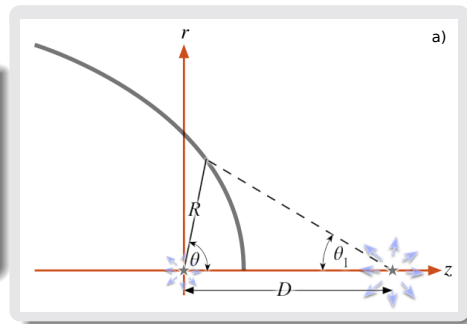
Where the algebraic form of these quantities for the ancantoid inner winds (without the "1" suffix) are described [▶ HERE](#). For the outer winds (suffix "1") (equations (12-15) and (19-22) of Cantó et al. (1996) click [▶ HERE](#)) and for the inner wind for the cantoid and wilkinoid case (equations (8-11) of Cantó et al. (1996), click [▶ HERE](#)



Discontinuity Contact Shape

An alternative form to get R is applying the sines law to the next triangle:

$$R = \frac{D \sin \theta_1}{\sin(\theta + \theta_1)}$$



Discontinuity Contact Shape

With this, we get trascendent equations for θ_1 . Then solve for $\theta_1(\theta)$ and finally get R:

Solution for Wilkinoids

For wilkinoids there is an explicit solution for $R(\theta)$:

$$R = R_0 \left[\csc^2 \theta (1 - \theta \cot \theta) \right]^{1/2}$$

Where:

$$R_0 = \left(\frac{\dot{M}_w^0 v_w}{4\pi \rho_a v_a^2} \right)^{1/2}$$

Where ρ_a and v_a are the density and velocity of the plane-parallel outer wind

For Cantoids

$$\theta_1 \cot \theta_1 - 1 = \beta (\theta \cot \theta - 1)$$

For ancantoids head

$$\theta_1 \cot \theta_1 - 1 = 2\beta I_k(\theta) \cot \theta - \frac{2\beta}{k+2} (1 - \cos^{k+2} \theta)$$

For ancantoids tail

$$\theta_1 \cot \theta_1 - 1 = 2\beta I_k(\pi/2) \cot \theta - \frac{2\beta}{k+2}$$

Discontinuity Contact Shape

Where:

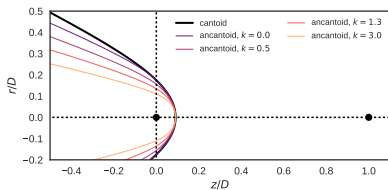
Ancantoids

$$\beta = 2(k+1) \frac{\dot{M}_w^0 v_w}{\dot{M}_{w1}^0 v_{w1}}$$

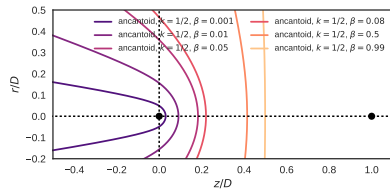
Cantoids

$$\beta = \frac{\dot{M}_w^0 v_w}{\dot{M}_{w1}^0 v_{w1}}$$

Fixed β

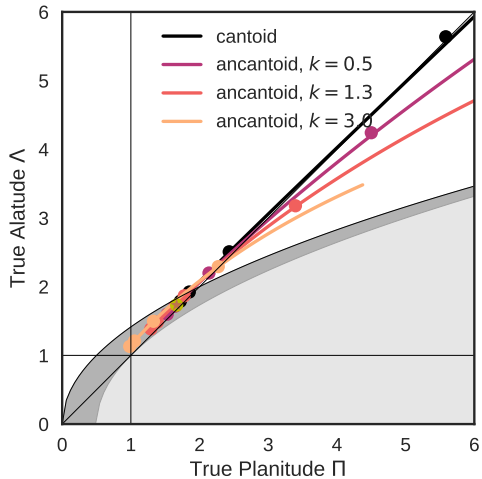


Fixed k



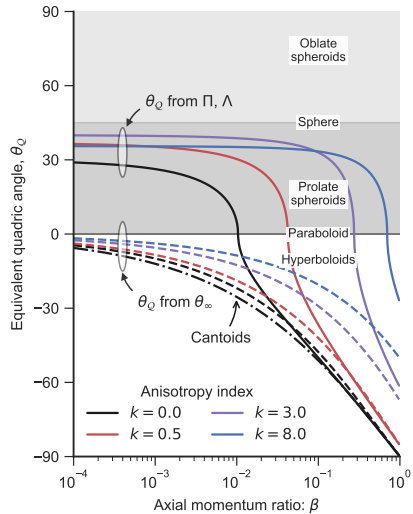
Planitude and alatitude

True Λ – Π diagram



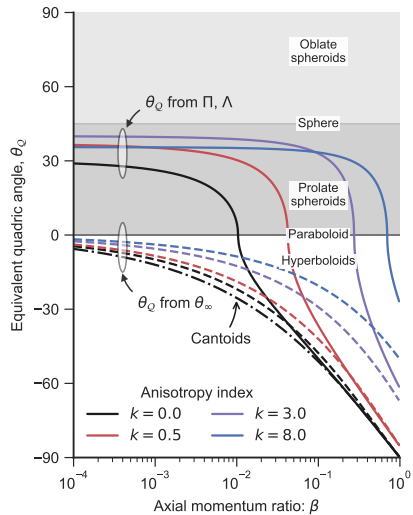
Thin Shell model fits to quadrics of Revolution

Once computed the planitude and alatitude, we may estimate the quadrics parameter Q or the equivalent θ_Q which approximates the shape of the bow shock head. As well the assymptotic angle θ_∞ is used to estimate the same parameters for the bow shock tail.



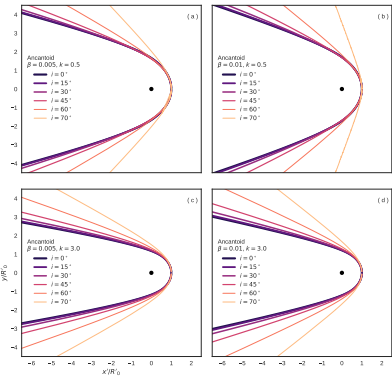
Thin Shell model fits to quadrics of Revolution

For a wide range of the anisotropy parameter k , for low β values the shape of the head fits with an ellipsoid and for higher β the head fits better with an hyperboloid. While the tail always fits with an hyperboloid. This will help us to understand the behavior of the apparent shape in a $\Lambda - \Pi$ diagram.



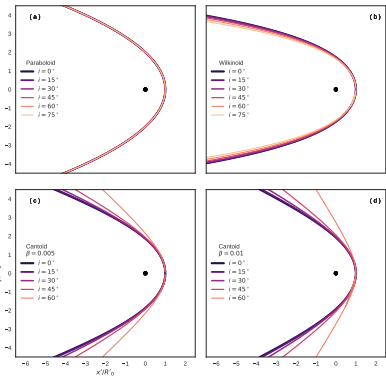
Projected Planitude and Alatitude

The apparent shape of multiple types of bow shocks becomes more open as the inclination increases. Because the tangent line shifts to the hyperbolic part of the bow shock (the tail) as the inclination increases.



Projected Planitude and Alatitude

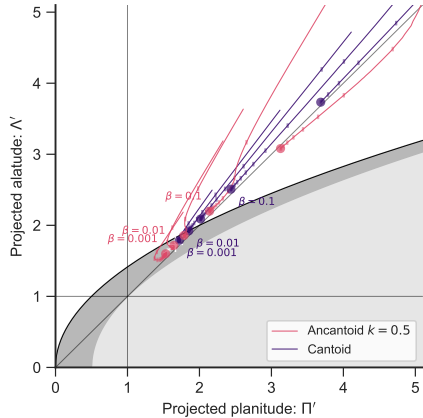
The wilkinoid is the exception of the rule (shape becomes closer with inclination). The confocal paraboloid ($\Pi = \Lambda = 2$) does not change with inclination (another shape not mentioned here is the trivial case of the confocal spheroid ($\Lambda = \Pi = 1$)).



Projected Planitude and Alatitude: $\Lambda - \Pi$ diagram

Main notes

The circle shows the shape of the bow shock in the body frame ($i = 0$) and the inclination grows along the curve. For low β the apparent shape changes from ellipsoid to hyperboloid.

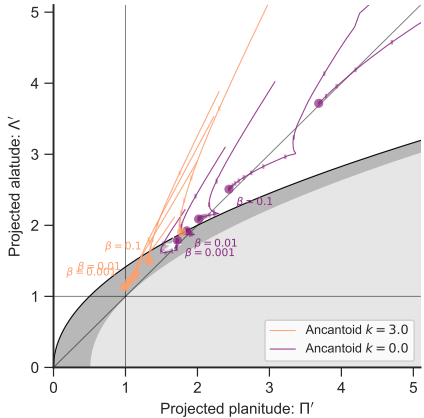


Projected Planitude and Alatitude: $\Lambda - \Pi$ diagram

Main notes

The ancantoids show a “kink” at an inclination such that the apparent apex passes through the inner wind discontinuity, where the second derivative of $R(\theta)$ has a slope deviation. This kink softens as the anisotropy parameter increases.

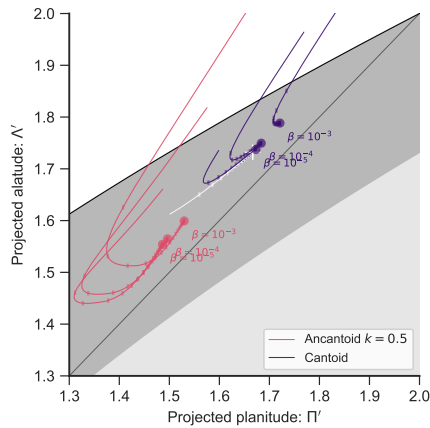
► Click [HERE](#)



Projected Planitude and Alatitude: Λ – Π diagram

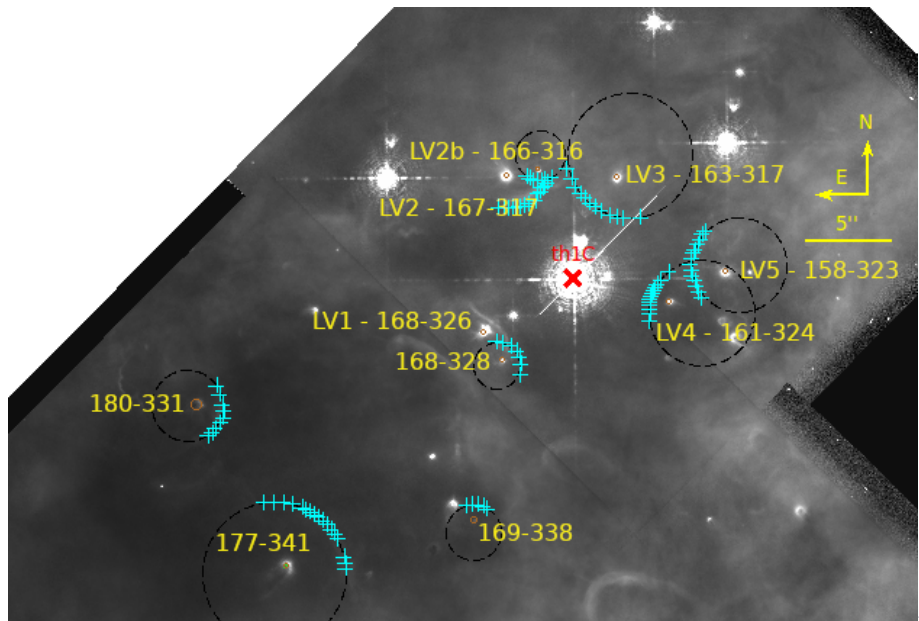
Main notes

The wilkinoid track does not show sustancial variations.



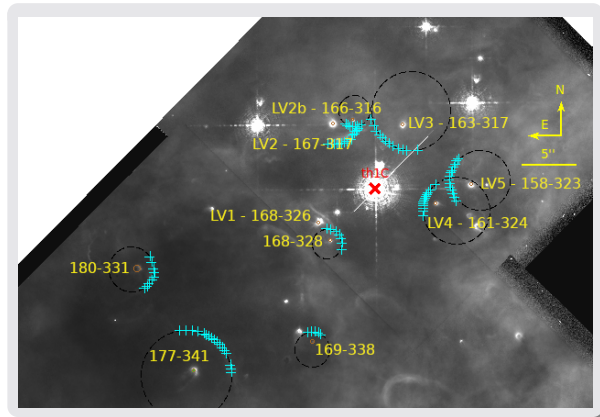
- [1] Introduction**
- [2] Bow Shocks in the ISM**
- [3] Orion Nebula**
- [4] Fundamental Concepts**
- [5] Thin Shell Model**
- [6] Results Obtained for the Classical Proplyds in Orion Nebula**
- [7] Summary and Conclusions**

The Trapezium observed with the HST



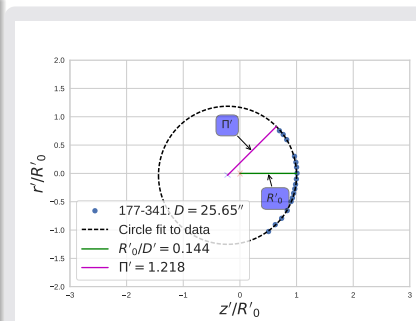
Obtaining the data

With DS9 tools, we get the coordinates (AR, DEC) of each proplyd (small circles), the position of θ^1 Ori C (red cross) and the position of each bow shock (cyan crosses).



Obtaining the data

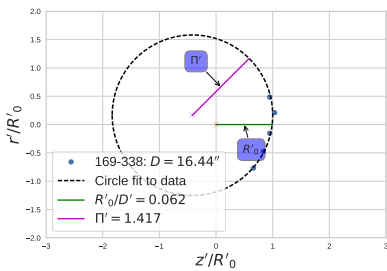
For each proplyd we measured the radius of curvature with a circular least square fit of the bow shock marks. R_0 is measured along the line between the proplyd and from the proplyd position to the resultant circle. And obtain with this the planitude. The alatitude is not available for any proplyd in the sample.



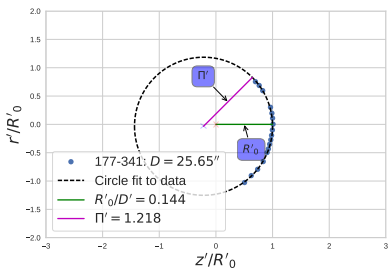
Obtaining the data

The number and spacing of the marks are proportional to the size of the bow shock and to our confidence in that we are tracing the bow shock correctly.

169-338



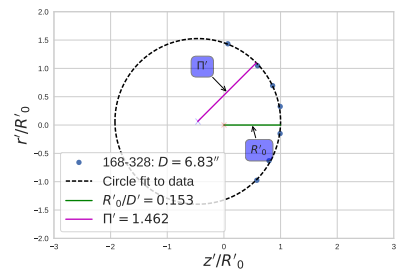
177-341



Sub-samples

For each proplyd, we did a set of sub-samples where we removed randomly about 1/3 of the marks (but left at least 4) and measure the planitude for each sub-sample. The deviation between sub-samples and the “main” measurement (without removing marks) measures the uncertainties of both the apparent apex radius and planitude.

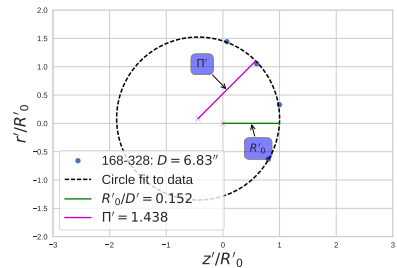
Main



Sub-samples

For each proplyd, we did a set of sub-samples where we removed randomly about 1/3 of the marks (but left at least 4) and measure the planitude for each sub-sample. The deviation between sub-samples and the “main” measurement (without removing marks) measures the uncertainties of both the apparent apex radius and planitude.

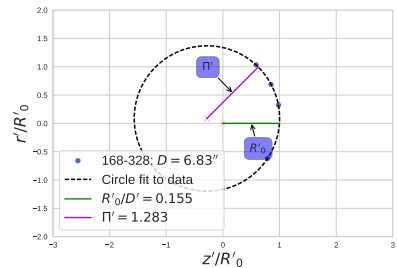
Sub-sample example



Sub-samples

For each proplyd, we did a set of sub-samples where we removed randomly about 1/3 of the marks (but left at least 4) and measure the planitude for each sub-sample. The deviation between sub-samples and the “main” measurement (without removing marks) measures the uncertainties of both the apparent apex radius and planitude.

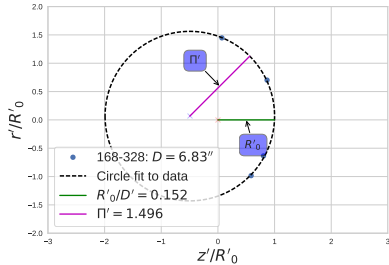
Sub-sample example



Sub-samples

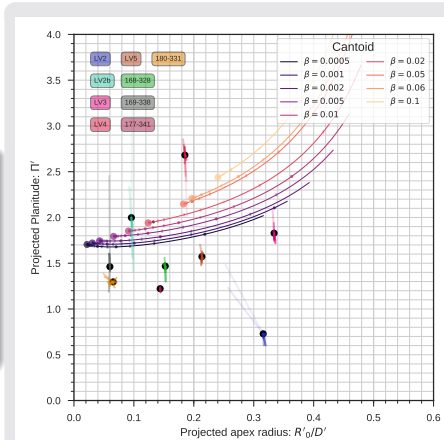
For each proplyd, we did a set of sub-samples where we removed randomly about 1/3 of the marks (but left at least 4) and measure the planitude for each sub-sample. The deviation between sub-samples and the “main” measurement (without removing marks) measures the uncertainties of both the apparent apex radius and planitude.

Sub-sample example



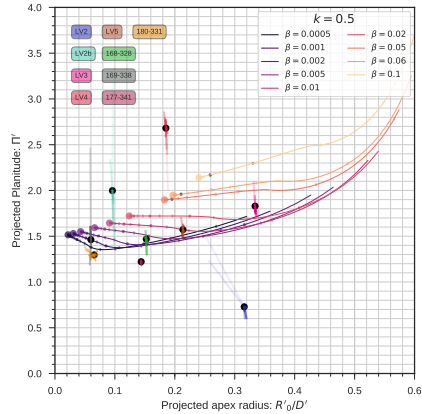
$\Pi - R_0/D$ diagram

Since the alatitude is not available for our set, we compare all the results in a $\Pi - R_0/D$ diagram against the thin shell model predictions, assuming a given anisotropy index k .



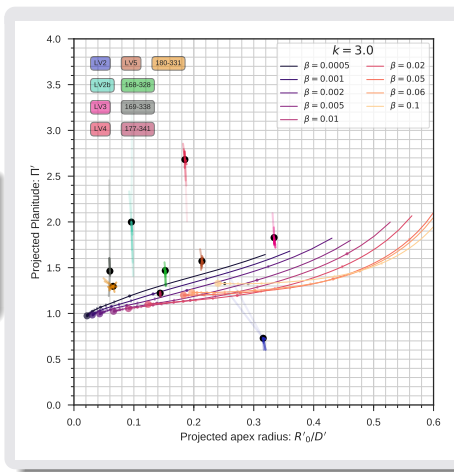
$\Pi - R_0/D$ diagram

For each prolyd, we may find multiple predictions for the winds momentum ratio β and inclination i for a given anisotropy index k by examining the intersections between the observations (black dots with radial uncertainty bars) and the thin shell model predictions (each curve has a fixed value of β and the inclination increases from left to right along each curve. Fixed intervals of i in degrees are shown).



$\Pi - R_0/D$ diagram

Each set of the parameters (k, β, i) allows to estimate the intrinsic distance D and the intrinsic apex radius R_0 .



Ionization and ram pressure balance

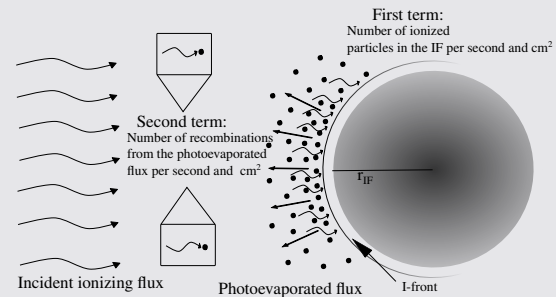
Having the true distance D estimated, we may evaluate ionization equilibrium in the photoevaporated flux.

Ionization equilibrium condition

$$F_* = u_{IF} n_{IF} + \omega r_{IF} \alpha'_{rec} n_{IF}^2$$

Ionizing flux from the star.

$$F_* = \frac{(1 - f_d) \mathcal{N}_*}{4\pi D^2}$$



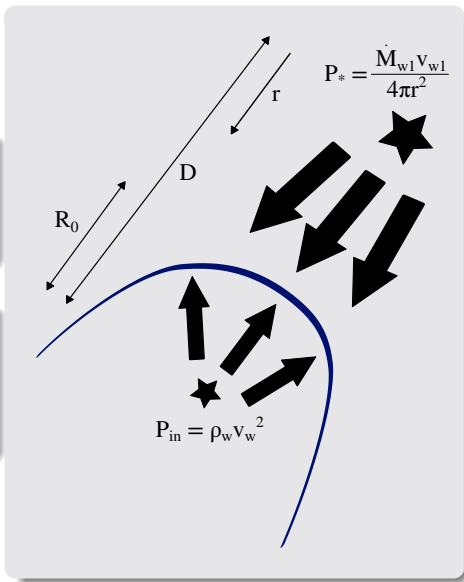
Ionization and ram pressure balance

Inner wind pressure in the shell.

$$P_{in} = \rho_{ps} v_w^2$$

Star's ram pressure

$$P_*(r) = \frac{\dot{M}_{w1} v_{w1}}{4\pi r^2}$$



θ^1 Ori C wind parameters

For the outer wind coming from θ^1 Ori C we have the observational constrain (García-Arredondo et al., 2001) that the ratio \dot{M}_{-7}/v_3 must be about 2. The two models which fullfill this condition are the following:

(García-Arredondo et al., 2002)

$$\begin{aligned}\dot{M}_{w1} &= 3.5 \times 10^{-7} M_{\odot} \text{ yr}^{-1} \\ v_{w1} &= 1200 \text{ km s}^{-1}\end{aligned}$$

This model fullfills the aditional constrain that $\dot{M}_{-7}v_3 = 4.2$.

(Gagné et al., 2005)

$$\begin{aligned}\dot{M}_{w1} &= 5.5 \times 10^{-7} M_{\odot} \text{ yr}^{-1} \\ v_{w1} &= 2760 \text{ km s}^{-1}\end{aligned}$$

These values are obtained with X-ray spectroscopy and MHD simulations.

Inner wind density

For the inner wind density we compare two assumptions. In both cases, we use the ionization front radius reported by García-Arredondo et al. (2001) but corrected by a factor of $\simeq 0.96$ due to the distance to orion nebula.

Importing ionization front densities from García-Arredondo et al. (2001)

Source	$r_{IF,14}$	N_6
168-328	2.7 ± 0.3	4.08 ± 0.48
169-338	2.7 ± 0.3	1.43 ± 1.09
177-314	19.6 ± 1.9	0.42 ± 0.06
180-331	11.7 ± 1.3	0.49 ± 0.08
LV2	7.6 ± 0.4	2.65 ± 0.23
LV2b	2.4 ± 0.6	4.21 ± 1.21
LV3	4.8 ± 0.7	3.19 ± 0.71
LV4	3.4 ± 0.3	4.21 ± 0.63
LV5	6.1 ± 0.7	2.37 ± 0.47

Derived from our estimations of β

We may derive the pre shock wind density as follows:

$$n_{ps} = \frac{\beta (\dot{M}_{w1} v_{w1})}{4\pi R_0^2 \mu m_H v_w^2}$$

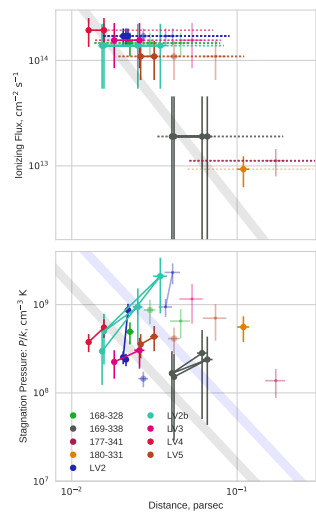
Where $\mu = 1.3$ for a gas with a sound speed of $\simeq 11 \text{ km s}^{-1}$. This assumption implies that pressure equilibrium is archived.

Ionization balance and ram pressure equilibrium

Importing inner wind densities from García-Arredondo et al. (2001)

Finally, for the inner wind velocity v_w we tried the range $M = [2, 3]$, where M is the Mach number of the inner wind: $M \equiv \frac{v_w}{c_{II}}$.

M=2

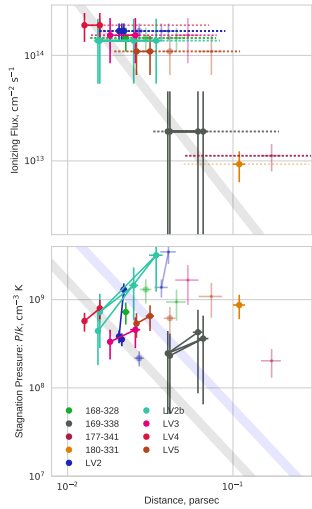


Ionization balance and ram pressure equilibrium

Importing inner wind densities from García-Arredondo et al. (2001)

Finally, for the inner wind velocity v_w we tried the range $M = [2, 3]$, where M is the Mach number of the inner wind: $M \equiv \frac{v_w}{c_{II}}$.

M=3

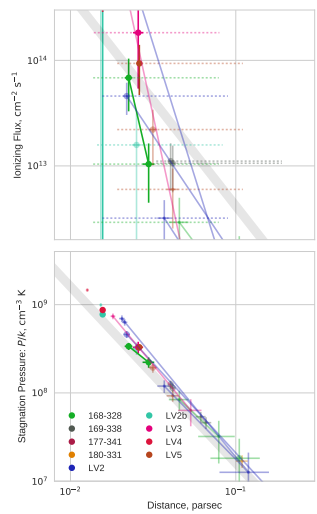


Ionization balance and ram pressure equilibrium

Derived inner wind density
from estimations of β

The gray line is the ram pressure of
 θ^1 Ori C obtained by
García-Arredondo et al. (2001,
2002)

M=2

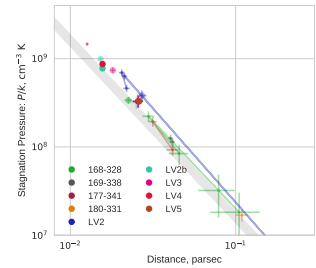
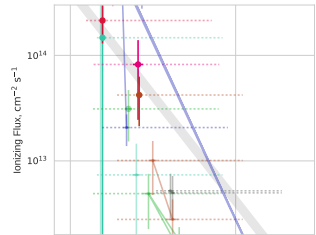


Ionization balance and ram pressure equilibrium

Derived inner wind density
from estimations of β

The gray line is the ram pressure of
 θ^1 Ori C obtained by
García-Arredondo et al. (2001,
2002)

M=3



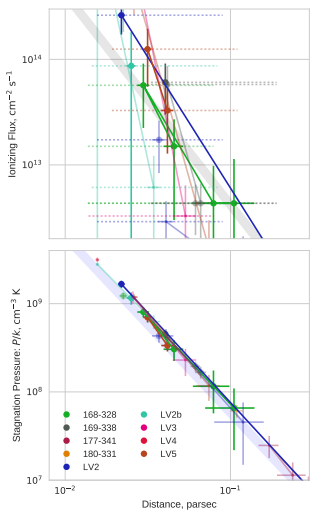
Ionization balance and ram pressure equilibrium

Derived inner wind density from estimations of β

The green line is the ram pressure of θ^1 Ori C obtained by Gagné et al. (2005)

Here we note how the ram pressure equilibrium assumption is accomplished.

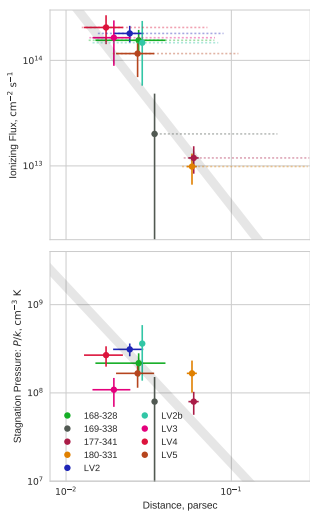
M=3



Ionization balance and ram pressure equilibrium

Finally, we compare with previous work (Henney & Arthur, 1998; García-Arredondo et al., 2001; Henney et al., 2002)

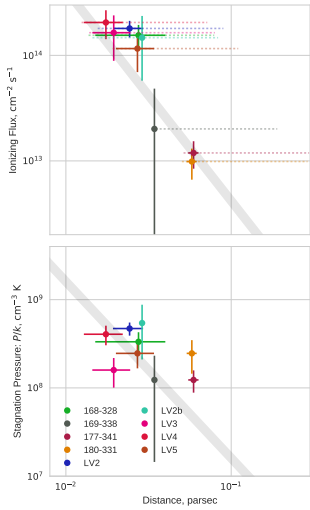
M=2



Ionization balance and ram pressure equilibrium

Finally, we compare with previous work (Henney & Arthur, 1998; García-Arredondo et al., 2001; Henney et al., 2002)

M=3



Future work

- For the Orion Nebula proplyds, improve methodology to obtain β and inclinations in order to get a better resolution in the (β, k, i) grid.
- Improve methodology to evaluate balance conditions.
- Develop other models where bow shocks occur besides the thin shell model (Henney et al. in prep)
- Apply the technique developed in this work to other classes of stellar bow shocks: OB runaway stars (Kobulnicky et al., 2016) and red giant and supergiant stars (Cox et al., 2012). And for LL objects in the outskirts of Orion Nebula (Henney et al., 2012).

- 1** Introduction
- 2** Bow Shocks in the ISM
- 3** Orion Nebula
- 4** Fundamental Concepts
- 5** Thin Shell Model
- 6** Results Obtained for the Classical Proplyds in Orion Nebula
- 7** Summary and Conclusions

Summary and conclusions

- The shape of an (ideally) cylindrically symmetric bow shock can be characterized by two adimensional parameters: the planitude Π and the alatitude Λ that can be obtained from theoretical models (such as the thin shell model but not restricted to) or observations.
- We develop a general method to find the projected shape (i.e, the limb brightened edge) or tangent line, described with the parameters (Π', Λ') , of a bow shock idealized as a cylindrical surface as a function of the inclination angle i .
- This method was applied to find inclination depending curves into the $\Lambda' - \Pi'$ plane for two sets of surfaces:
 - **Quadric surfaces**, which are the surfaces of revolution of the conic sections.
 - The solutions of the **Thin Shell Model** (Cantó et al., 1996)

Summary and Conclusions

- We apply this work to the bow shocks observed in the core of the Orion Nebula due to the wind-wind interaction between proplyd's photoevaporated flow and θ^1 Ori C wind.
- We measured the projected distance D' to θ^1 Ori C for a set of proplyds and the projected planitude Π' of their respective bow shock. The projected alatitude was not measured due to the decay of emmision with θ .
- We compared visually each measurement of planitude against the thin shell model predictions. Assuming a given anisotropy index k , we obtain may plausible values for the inclination and the winds momentum ratio β , leading us to estimate the intrinsic dimensions of each bow shock and the intrinsic distance to θ^1 Ori C.

Summary and conclusions

- We evaluated ionization balance and ram pressure balance under certain assumptions about θ^1 Ori C wind properties.
- We assumed that the photoevaporated flow velocity lies in the range $M = [2, 3]$, we didn't see substantial changes in both balance conditions.
- We compared two different estimations of the photoevaporated flow density and evaluated balance conditions, but we lack of an appropriate method to determine which approximation is better (or if none of them is).



*Thank you for
coming today*

References I

- Bally J., Sutherland R. S., Devine D., Johnstone D., 1998, AJ, 116, 293
- Bertoldi F., 1989, ApJ, 346, 735
- Bertoldi F., McKee C. F., 1990, ApJ, 354, 529
- Cantó J., Raga A. C., Wilkin F. P., 1996, ApJ, 469, 729
- Cox N. L. J., et al., 2012, A&A, 537, A35
- Daley-Yates S., Stevens I. R., 2018, MNRAS, 479, 1194
- Gagné M., Oksala M. E., Cohen D. H., Tonnesen S. K., ud-Doula A., Owocki S. P., Townsend R. H. D., MacFarlane J. J., 2005, ApJ, 628, 986
- García-Arredondo F., Henney W. J., Arthur S. J., 2001, ApJ, 561, 830
- García-Arredondo F., Arthur S. J., Henney W. J., 2002,
Revista Mexicana de Astronomía y Astrofísica, 38, 51
- Gfrerrer A., Zsombor-Murray P., 2009, Journal for Geometry and Graphics, 13, 131–144

References II

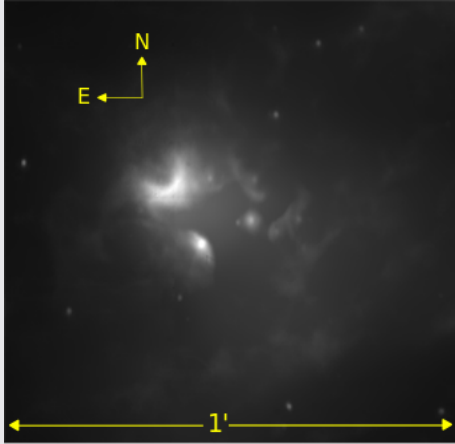
- Goldman R., 1983, IEEE Computer Graphics and Applications, 3, 68–76
- Gutiérrez-Soto L., 2015, Master's thesis, Universidad Nacional Autónoma de México
- Henney W. J., Arthur S. J., 1998, AJ, 116, 322
- Henney W. J., O'Dell C. R., Meaburn J., Garrington S. T., Lopez J. A., 2002, ApJ, 566, 315
- Henney W. J., García-Díaz M. T., O'Dell C. R., Rubin R. H., 2012, Monthly Notices of the Royal Astronomical Society, 428, 691
- Johnstone D., Hollenbach D., Bally J., 1998, ApJ, 499, 758
- Kobulnicky H. A., et al., 2016, ApJS, 227, 18
- Menten K. M., Reid M. J., Forbrich J., Brunthaler A., 2007, A&A, 474, 515
- Perley R. A., Dreher J. W., Cowan J. J., 1984, ApJ, 285, L35
- Roberto M., et al., 2005, AJ, 129, 1534

References III

- Tarango Yong J. A., Henney W. J., 2018, MNRAS, 477, 2431
- Tsamis Y. G., Flores-Fajardo N., Henney W. J., Walsh J. R.,
Mesa-Delgado A., 2013, MNRAS, 430, 3406

MPAQ (Most Probably Asked Questions)

Just in case slides



The trapezium region at $10 \mu\text{m}$ by Roberto et al. (2005)

[Return Button](#)

Planitude and Alatitude: Algebraic expressions

Planitude

$$\Pi = \frac{R_0}{R_0 - R_{\theta\theta,0}}$$

Where $R_{\theta\theta,0}$ is the second derivative of R at the apex.

Alatitude

$$\Lambda = \frac{R(\pi/2)}{R_0}$$

► Return Button

Quadrics of Revolution: Parametrization

Parametrization

$$x = x_0 + \sigma a \mathcal{C}(t)$$

$$y = b \mathcal{S}(t)$$

$$\tan \theta = \frac{b \mathcal{S}(t)}{x_0 + \sigma a \mathcal{C}(t)}$$

$$R = \left[(x_0 + \sigma a \mathcal{C}(t))^2 + b^2 \mathcal{S}^2(t) \right]^{1/2}$$

▶ Return Button

where:

$$t \forall \mathbb{R}$$

$$\mathcal{C}(t), \mathcal{S}(t) = \begin{cases} \cos t, \sin t & \text{ellipses} \\ \cosh t, \sinh t & \text{hyperbolas} \end{cases}$$

$$\sigma = \begin{cases} +1 & \text{ellipses} \\ -1 & \text{hyperbolas} \end{cases}$$

$$x_0 = R_0 - \sigma a$$

Useful Matrices

$$A_x(\phi) = \begin{pmatrix} 1 & 0 & 0 \\ 0 & \cos \phi & -\sin \phi \\ 0 & \sin \phi & \cos \phi \end{pmatrix}$$

$$A_y(i) = \begin{pmatrix} \cos i & 0 & -\sin i \\ 0 & 1 & 0 \\ \sin i & 0 & \cos i \end{pmatrix}$$

► Return Button

Useful unitary vectors

$$\hat{t}_0 = \begin{pmatrix} -\cos \alpha \\ \sin \alpha \\ 0 \end{pmatrix}$$

$$\hat{t} = A_x(\phi) \hat{t}_0 = \begin{pmatrix} -\cos \alpha \\ \sin \alpha \cos \phi \\ \sin \alpha \sin \phi \end{pmatrix}$$

$$\hat{n}_0 = \begin{pmatrix} \sin \alpha \\ \cos \alpha \\ 0 \end{pmatrix}$$

$$\hat{n} = A_x(\phi) \hat{n}_0 = \begin{pmatrix} \sin \alpha \\ \cos \alpha \cos \phi \\ \cos \alpha \sin \phi \end{pmatrix}$$

$$\hat{x}' = A_y(-i) \begin{pmatrix} 1 \\ 0 \\ 0 \end{pmatrix}$$

$$\hat{y}' = A_y(-i) \begin{pmatrix} 0 \\ 1 \\ 0 \end{pmatrix}$$

$$\hat{z}' = A_y(-i) \begin{pmatrix} 0 \\ 0 \\ 1 \end{pmatrix}$$

► Return Button

Projected Alatitude and Planitude

$$R'_0 = R(\theta_0) \cos(\theta_0 - |i|)$$

Projected alatitude

$$R'_{90} = R(\theta_{90}) \sin \theta_{90} (1 - \sin^2 \phi_T(\theta_{90}))^{1/2}$$

Where:

$$\cot \theta_{90} = \frac{1 - (1 + \omega(\theta_{90})^2 \sin^2 2i)^{1/2}}{2\omega(\theta_{90}) \cos^2 i}$$

$$\text{Finally } \Lambda = R'_{90}/R'_0$$

projected planitude

$$\Pi' = \frac{R'_0}{R'_0 - R_{\theta' \theta', 0}}$$

► Return Button

Projected Shape of Quadrics of Revolution

In terms of (a, b, t)

$$x'_T = \frac{\mathcal{C}(t)}{a \cos i} (a^2 \cos^2 i + \sigma b^2 \sin^2 i) + x_0 \cos i$$

$$y'_T = b \mathcal{S}(t) \left(1 - \frac{b^2 \mathcal{C}^2(t)}{a^2 \mathcal{S}^2(t)} \tan^2 i \right)^{1/2}$$

In terms of (a', b', t')

$$\begin{aligned} x'_T &= a' \mathcal{C}(t') + x'_0 \\ y'_T &= b' \mathcal{S}(t') \end{aligned}$$

Where:

$$a' = a \cos i f_{Q,i}$$

$$b' = b$$

$$\mathcal{C}(t') = f_{Q,i} \mathcal{C}(t)$$

$$f_{Q,i} = (1 + Q \tan^2 i)^{1/2}$$

With this we show that the projected shape of a quadric is another quadric of the same type. The particular case of the paraboloid is shown [HERE](#).

Paraboloid

In the parametric equations for the paraboloid, we assume that we know the planitude Π .

[Return Button](#)

Intrinsic Shape

$$x/R_0 = 1 - \frac{1}{2}\Pi t^2$$

$$y/R_0 = \Pi t$$

Apparent shape in terms of (t, Π)

$$x'_T/R_0 = \cos i \left[1 + \frac{1}{2}\Pi t \tan^2 i - \frac{1}{2}\Pi (t^2 - \tan^2 i) \right]$$

$$y'_T/R_0 = \Pi (t^2 - \tan^2 i)^{1/2}$$

Apparent shape in terms of (t', Π')

$$x'_T/R'_0 = 1 - \frac{1}{2}\Pi' t'^2$$

$$y'_T/R'_0 = \Pi' t'$$

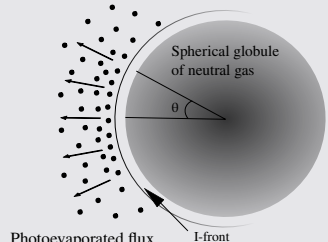
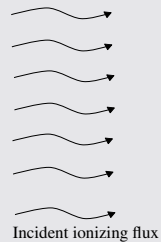
where:

$$t' = \cos i (t^2 - \tan^2 i)^{1/2}$$

$$\Pi' = \frac{2\Pi}{2 \cos^2 i + \Pi \sin^2 i}$$

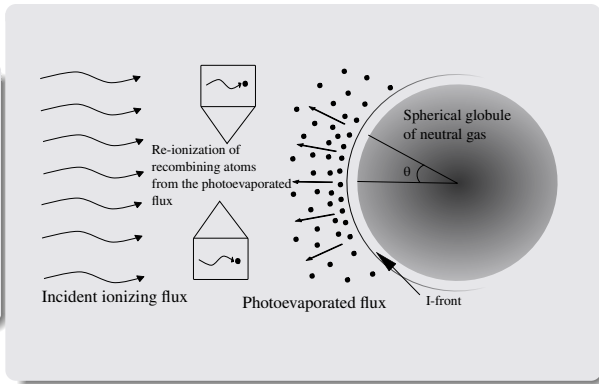
Anisotropy index for proplyds

Let us consider a globule of neutral gas irradiated by a plane-parallel ionizing radiation field from a distant source forming a ionization front and a photoevaporated flux of ionized gas.



Anisotropy index for proplyds

A fraction of the incident flux is absorbed for recombined atoms (to all states except ground state) from the photoevaporated flux itself.



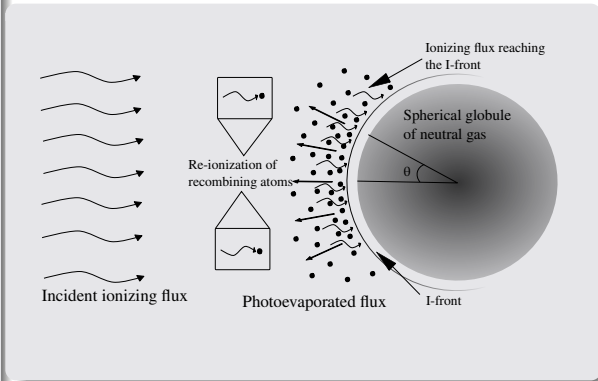
Anisotropy index for proplyds

The ionizing flux that actually reaches the ionizing front and evaporates new material from the globule as a function of the polar angle θ is given by (Bertoldi, 1989):

$$F_{II}(\theta) = F_{II}(0) \cos^{\beta} \theta$$

Where:

$$\beta \simeq - \left(2 + \frac{1.53}{q - \phi_q} \right)^{-1}$$



Anisotropy index for proplyds

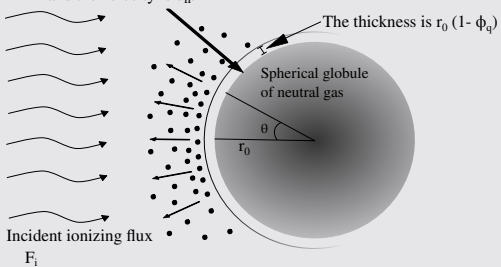
q is the ratio between the ionizing radiation flux and the flux of ionized gas streaming off the the ionization front.

And ϕ_q is a measure of the thickness of the ionization front.

The density here is n_I and the velocity is u_{IF}

$$q = \frac{F_i}{n_I u_{IF}}$$

The thickness is $r_0 (1 - \phi_q)$



Anisotropy index for proplyds

The extreme case $q \gg 1$ implies that most of the incident radiation is absorbed when re-ionizing the recombining gas and only a small fraction reaches the ionizing front and ionizes the neutral gas. In this case we have a thin ionization front, so we have $\phi_q \simeq 1$. That implies that $\beta \simeq -1/2$. In the other extreme case $q \ll 1$ we have $q \simeq \phi_q$ that implies $\beta \simeq 0$.

▶ Return Button

Anisotropy index for proplyds

Finally, equation (3.4) from Bertoldi & McKee (1990) implies that:

$$\begin{aligned} n(\theta) &\propto F_{II}(\theta) \cos \theta \\ \implies n(\theta) &\propto \cos^{\beta+1} \theta \end{aligned}$$

▶ Return Button

MLR, momentum and angular momentum rates for ancantoid inner winds

$$\dot{M}_w = \dot{M}_w^0 (1 - \cos^{k+1} \theta)$$

Where \dot{M}_w^0 is the mass loss rate integrated over all the range of θ .

$$\dot{\Pi}_{wz} = \frac{\dot{M}_w^0 v_w (k + 1)}{k + 2} \max(1 - \cos^{k+2} \theta, 1)$$

$$\dot{\Pi}_{wr} = \frac{1}{2} \dot{M}_w^0 v_w I_k(\theta)$$

$$\dot{\mathbf{J}}_w = 0$$

$$I_k(\theta) = \int_0^{\max(\theta, \pi/2)} \cos^k \theta \sin^2 \theta \, d\theta$$

► Return Button

MLR, momentum and angular momentum rates for cantoid and wilkinoid inner winds

$$\dot{M}_w = \frac{\dot{M}_w^0}{2} (1 - \cos \theta)$$

Where \dot{M}_w^0 is the mass loss rate integrated over all the range of θ .

$$\dot{\Pi}_{wz} = \frac{\dot{M}_w^0 v_w}{4} \sin^2 \theta$$

$$\dot{\Pi}_{wr} = \frac{\dot{M}_w^0 v_w}{4} (\theta - \sin \theta \cos \theta)$$

$$\dot{J}_w = 0$$

▶ Return Button

MLR, momentum and angular momentum rates for the outer wind

Cantoid and Ancantoid

$$\dot{M}_{w1} = \frac{\dot{M}_w^0}{2} (1 - \cos \theta_1)$$

Where \dot{M}_w^0 is the mass loss rate integrated over all the range of θ .

$$\dot{\Pi}_{wz1} = -\frac{\dot{M}_w^0 v_{w1}}{4} \sin^2 \theta_1$$

$$\dot{\Pi}_{wr1} = \frac{\dot{M}_w^0 v_{w1}}{4} (\theta_1 - \sin \theta_1 \cos \theta_1)$$

$$\dot{J}_{w1} = \frac{\dot{M}_w^0 v_{w1}}{4} (\theta_1 - \sin \theta_1 \cos \theta_1) D$$

Wilkinoid

$$\dot{M}_{w1} = \pi \rho_a v_a R^2 \sin^2 \theta$$

$$\dot{\Pi}_{wz1} = -\pi \rho_a v_a^2 \sin^2 \theta$$

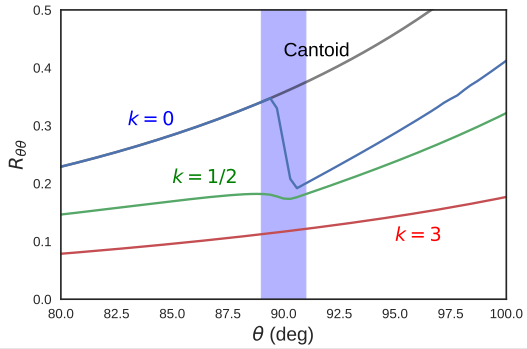
$$\dot{\Pi}_{wr1} = 0$$

$$\dot{J}_{w1} = \frac{2}{3} \pi \rho_a v_a^2 R^3 \sin^3 \theta$$

► Return Button

$R_{\theta\theta}(\theta)$ vs θ

When the inclination is such that the apparent apex passes through the shaded zone, the “kink” of the planitude appears



► Return Button